Thermochemical solar-driven reduction of CO2 into separate streams of CO and O2 via an isothermal oxygen-conducting ceria membrane reactor

Stéphane Abanades, Anita Haeussler, Anne Julbe

Thermochemical solar-driven reduction of CO_2 into separate streams of CO and O_2 via an isothermal oxygen-conducting ceria membrane reactor

Stéphane ABANADES [a] *, Anita HAEUSSLER [a], Anne JULBE [b]

[a] Processes, Materials and Solar Energy Laboratory, CNRS-PROMES, 7 Rue du Four Solaire, 66120 Font-Romeu, France

[b] Institut Européen des Membranes, IEM, UMR-5635, ENSCM, CNRS, Univ Montpellier, Place Eugène Bataillon, 34095 Montpellier cedex 5, France

* Corresponding author: Tel +33 (0)4 68 30 77 30

E-mail address: stephane.abanades@promes.cnrs.fr

Abstract: CO_2 single-step thermolysis was achieved using oxygen permeable MIEC (mixed ionic-electronic conducting) membranes made of ceria for separate production of CO on the feed side and O_2 on the sweep side. The CO_2-dissociation reaction was driven by concentrated solar energy as a renewable thermal energy source and by applying a chemical potential gradient between both membrane sides. A continuous oxygen transfer across the membrane was achieved thanks to a flow of inert gas on the permeate side. This created the required oxygen partial pressure gradient and favored oxygen permeation via oxygen ion diffusion through the ceria membrane thickness. A novel solar chemical reactor integrating the reactive ceria membrane was designed and tested under real concentrated solar radiation, with operating temperatures up to 1550°C. The reactive part of the tubular redox membrane was

located inside a well-insulated cavity receiver for homogeneous heating, which was fed with a carrier argon flow on the sweep side to facilitate the transport and removal of the permeated oxygen. The dynamic response of the solar fuel production upon changing the operating conditions (temperature, CO_2 mole fraction, and feed gas flow rate) in the membrane reactor was investigated by quantifying the evolved gas production rates. Continuous CO_2 dissociation was achieved on the feed side inside the tubular membrane with *in-situ* spatial separation of O_2 and CO streams across the membrane. Reliable solar membrane reactor operation under real concentrated sunlight was successfully demonstrated for the first time, with stable and unprecedented CO production rates up to 0.071 μmol/cm^2/s at 1550°C and CO/O_2 ratio of 2.

Keywords: solar reactor, ceramic membrane, oxygen transport, ceria, MIEC, CO_2 dissociation, solar fuel

1. Introduction

The development of sustainable, low cost, and efficient technology for the conversion of CO_2 into fuels is of major concern to face the problems of global warming and depletion of carbon-based energy resources. The utilization of CO_2 as a chemical feedstock to produce synthetic fuels is a great opportunity to consider CO_2 as a resource that can be recycled rather than a waste with a cost of disposal [1-2]. Therefore, CO_2 could be a raw material feedstock of nearly zero cost for conversion to chemical synthetic fuels. The sources of CO_2 are varied and boundless (power plants, refineries, cement works, etc.), and the solar recycling of

captured CO_2 is a novel alternative option to underground CO_2 sequestration. The proposed CO_2-recycling solar process can thus be implemented to compensate and counterbalance the growing CO_2 emissions associated with the transportation sector.

The use of thermal energy derived from concentrated solar radiation to split CO_2 (or H_2O) has potential advantages over other photobiological, photochemical or electrochemical conversion methods because of its scalability and theoretical high efficiency, without any precious metal catalyst [3-6]. Photo/electrochemical dissociation of H_2O or CO_2 suffers from low conversion yields and requires precious catalysts [7]. The electrochemical process is neither economical nor efficient for large-scale production, because the required intermediate electricity production penalizes the overall solar-to-fuel energy conversion efficiency, even if electricity comes from renewable energies (e.g. photovoltaics or concentrated solar power). In contrast, solar thermal processes inherently operate at high temperatures, avoid the costly solar-to-electric conversion, and utilize the entire solar spectrum. As such, they provide a thermodynamically favourable path to solar fuels production with potentially high solar-to-fuel energy conversion efficiency. The splitting of CO_2 (or H_2O) via thermochemical cycles is advantageous because it divides an unfavourable reaction (direct thermolysis of CO_2 or H_2O) into two steps that are thermodynamically more favourable [8].

The considered redox materials are commonly non-stoichiometric oxides including ceria-based fluorite systems ($CeO_{2-\delta}$) and perovskites ($ABO_{3-\delta}$) [9-10]. These oxides are not consumed but entirely recycled in the cyclic process. For such non-stoichiometric oxides, the reduction step proceeds in solid state via oxygen diffusion and formation of oxygen vacancies in the oxide lattice that are exploited for capturing oxygen from H_2O and CO_2 to produce H_2 and CO. In this case, oxygen-deficient materials are formed and the oxide non-stoichiometry δ is fixed by the reaction conditions (temperature, O_2 partial pressure), which determines the

amount of produced fuel [11]. The syngas (H_2/CO) can be further converted to various liquid hydrocarbon fuels via existing catalytic processes (e.g. Fischer-Tropsch reaction).

Alternatively, the CO_2 (or H_2O) thermolysis reaction can be achieved by using oxygen-conducting membranes for *in-situ* separation of CO (or H_2) and O_2 via direct oxygen ion permeation through the redox membrane [12-16]. In this case, an oxygen partial pressure gradient is applied between both sides of the membrane. This facilitates the oxygen transfer across the membrane from the CO_2 feed side to the sweep side for continuous oxygen removal by the carrier inert gas. The flow of inert gas on the sweep side allows decreasing the oxygen partial pressure at the membrane surface, thus promoting oxygen desorption. Continuous CO_2 splitting into CO and O_2 can thus be achieved isothermally with *in-situ* physical separation of products streams by the membrane, thereby avoiding recombination issues [14-16].

Recently, a reactor using ceria reactive membrane was developed where the radiation from a solar simulator directly heated an alumina tube in which the ceria tubular membrane was placed vertically [17-18]. CO_2 was injected inside the tube and Ar swept the outside to remove the oxygen transferred through the reactive membrane. The oxygen vacancies created in the membrane were re-filled by the oxygen brought by CO_2, thus producing CO. The highest CO production rate of 0.024 µmol/cm^2/s was achieved at 1600°C under p_{O_2}= 3x10^{-6} bar [17]. In another study, the co-production of both H_2 and CO using a similar reactive membrane was investigated [18]. At steady state with a temperature of 1600°C under p_{O_2}=0.2 Pa, the fuel production rate reached 0.038 µmol/cm^2/s. In the field of ceramic membranes, perovskite materials have been previously developed as oxygen or hydrogen separation membranes to conduct oxygen ions or protons, and have been widely applied for methane reforming in the range 600-1000°C [19-24]. Hydrogen production was also often considered with reducing agents such as CH_4 (or even H_2 itself [22]) to promote the oxygen

consumption on the sweep side (e.g. by reacting with CH_4 according to the partial oxidation reaction of methane, POM) [25-29]. The use of oxygen-permeable membranes for direct CO_2 (or H_2O) splitting above 1000°C is still sparsely advanced and solar-driven membrane reactors have never been studied and demonstrated so far.

The aim of this study was to develop a new solar membrane reactor with real on-sun demonstration and performance evaluation. In a previous work, a monolithic solar reactor was developed for integrating the reactive materials as porous media (such as foams acting as porous volumetric solar absorbers) with interconnected network of macropores and high surface area available for solid-gas reactions [30-31]. Heterostructures composed of perovskite coating on a ceria foam substrate were also considered, as well as microstructured biomimetic ceria [32-33]. During reactor operation, the material was first thermally activated by increasing the solar receiver temperature, delivering oxygen from its lattice and creating oxygen vacancies. Then, the H_2O or CO_2 stream flowing inside the ceramic structure oxidized the reduced activated material, while producing pure H_2 or CO, and allowing cyclic operation in a single reactor. The two-step process could thus be carried out in the same reactor with temperature-swing redox cycling. Under appropriate conditions, both steps occurred with high rates and efficiencies for rapid reaction kinetics and without any deactivation of the material between steps. There are still key challenges to enhance the overall system energy efficiency. These challenges and limitations are related both to discontinuous fuel production due to temperature swing operations and to heat recovery (solid and gas phases) required between the two steps.

Alternatively, a different operating mode based on oxygen partial pressure gradient between the two reaction compartments separated by a semi-permeable oxygen membrane has been developed in this work (Figure 1). The main advantage of such a reaction scheme, using reduced O_2 partial pressure, lies on the possibility to run this process in isothermal and

continuous conditions, using a membrane reactor. The redox reactions can thus be carried out simultaneously at the same temperature, in two distinct compartments separated by the dense mixed-ion-electron-conducting (MIEC) membrane able to transport the charge carriers (oxygen, vacancies, electrons) through the bulk via a thermally activated process. The mixed ionic-electronic conduction in such materials at high temperatures avoids the application of an external electrical supply for electronic transfer. This kind of reactor concept results in concomitant production of O_2 and H_2/CO, obtained in separate streams. Consequently, the same outputs as electrolysis can be reached by the membrane process, but without requiring any electrical power supply.

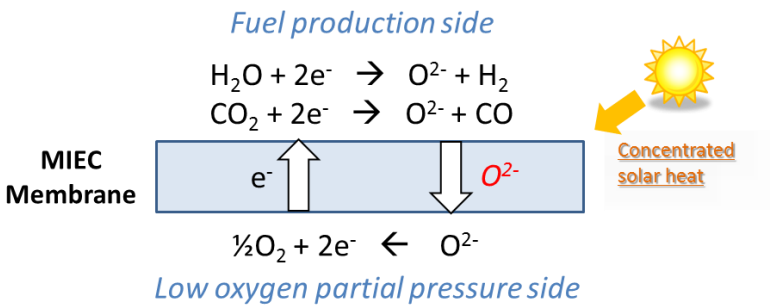

Figure 1: Operation principle of the reactive ceramic oxide membrane reactor: schematic of oxygen ions and electrons transport across the membrane (isothermal and continuous process operation).

This study demonstrates for the first time the potential of such an isothermal membrane solar reactor based on oxygen ion-conducting materials for oxygen transport and continuous fuel production via high-temperature thermochemical process. Accordingly, ceria was selected as the reactive membrane material due to its attractive redox properties, thermal stability and high capabilities in oxygen storage and mobility [11, 13]. Diffusion of oxygen in ceria occurs via ambipolar diffusion of both electrons and ions, and the formation of oxygen vacancies when

increasing the temperature results in high oxygen diffusion coefficients. Actually, the involved redox reactions on each side of the membrane based on Ce^{4+}/Ce^{3+} redox pair can be written as:

Oxidation side: $2Ce^{3+} + CO_2 \rightarrow 2Ce^{4+} + CO + O^{2-}$ (1)

Reduction side: $2Ce^{4+} + O^{2-} \rightarrow 2Ce^{3+} + ½\ O_2$ (2)

The global reaction (1)+(2) thus corresponds to the single-step CO_2 thermolysis (3):

$$CO_2 \rightarrow CO + ½\ O_2 \quad (3)$$

For such a dense redox membrane, oxygen ions are transported via diffusion through vacancies in the crystal lattice and are the only permeating species (complete selectivity for oxygen transport). As such, the required driving force for bulk species transport through the ceria membrane can be sustained by coupling the two different reactions in a single membrane reactor, while applying an O_2 partial pressure gradient between the two membrane sides. This can be achieved either via inert sweep gas in the low oxygen partial pressure side (p_{O2}~10^{-5} bar) or via a reduction of the overall pressure. The latter option requires fully dense and perfectly sealed membranes to avoid any transfer of molecular gas species. This study aims to examine the influence of the main operating conditions of the membrane reactor on fuel yield and CO_2-splitting performance, in order to provide a first proof-of-concept of the developed solar technology. The membrane-driven thermolysis process was integrated and demonstrated for the first time in a real solar reactor, yielding remarkable fuel production performance under continuous and isothermal operation up to 1550°C.

2. Solar membrane reactor

This study aimed to construct and equip at lab-scale a ceramic membrane reactor and to demonstrate its efficiency for high-temperature isothermal splitting of CO_2. The membrane reactor, with 2 separate compartments allows carrying out simultaneously the high temperature reduction of the MIEC oxide material on one side of the membrane, while the CO_2-splitting reaction, inserting oxygen species in the MIEC lattice, is operated on the other side.

The novel solar reactor (Figure 2) consists of an insulated cavity-receiver in which a tubular membrane (dead-end tube, finger type) made of ceria is inserted horizontally. The use of a cavity approaching blackbody absorber allows for better control of both temperature stability and homogeneity along the tube. This cavity (80 mm height and 60/50 mm out/in diameters) made of alumina is closed at the top by an alumina front cover with a small aperture (18 mm diameter) used for the access of concentrated solar radiation. A board of zirconia felt (2 mm thick) insulates the alumina cover, thereby reducing the radiative losses at the upper front and the cavity is insulated by a surrounding porous alumino-silicate fibrous layer. The top of the reactor is closed by a transparent glass window to operate in controlled atmosphere.

When targeting isothermal operation for the membrane reactor, the same temperature is applied for both reaction steps. Although isothermal operation is pursued, a weak temperature gradient may exist between the two membrane sides because only one face can be irradiated by solar energy. Consequently, the thermally-favoured reduction reaction was carried out on the irradiated membrane side where the maximum temperature is expected.

The inert gas Ar (99.9999% purity, $[O_2]<2$ ppm) is supplied to the outer side of the membrane (sweep reduction side) to control the oxygen partial pressure in the cavity. It enters the cavity via the aperture. CO_2 (99.995% purity) is supplied to the inner side of the membrane (oxidation side) via a small inlet alumina pipe (6x4 mm) inserted inside the membrane tube. CO_2 exits near the membrane closed extremity and backflows in the annular space between

the feeding pipe and the inner membrane wall, thus enabling suitable solid/gas contact on the whole length of the membrane surface. Both membrane sides are operated at slightly above atmospheric pressure (0.9 bar) using a mechanical pressure regulator to avoid any transfer of molecular gaseous species that may arise from leakage. Three pressure transmitters measure the pressure at the gas inlets and in the reactor cavity to control pressure equilibrium between both membrane sides. The gas flow rates are regulated with mass-flow controllers (MFC, Brooks Instruments model SLA5850S).

The reactor temperature is measured at different locations with B-type thermocouples (T1 to T4, T1 is located just below the membrane on the outer side, T4 is placed inside the tubular membrane between the central feeding pipe and the inner membrane side, T2 is in contact with the cavity wall, and T3 is at the cavity bottom) and by a solar-blind pyrometer (operating at 4.8-5.2 μm) directly pointing at the membrane outer surface.

The prototype membrane reactor is installed at the focus of a vertical-axis solar furnace comprising a sun-tracking heliostat and a parabolic dish solar concentrator (2 m-diameter, focal point at 0.85 m ahead of the parabolic mirror) located at the solar facilities of PROMES-CNRS laboratory. The focal point is located at the cavity aperture for maximum solar radiation absorption inside the cavity receiver. The reactor temperature is controlled and adjusted by means of an intermediate shutter, enabling heating/cooling rates and temperature control.

The O_2 released by the membrane on the outer side is continuously evacuated from the cavity by the Ar carrier gas flow. The reactor is heated up to the desired temperature while a trace O_2 analyzer with electrochemical cell (Systech, range from 0.1 ppm to 1%, precision ±2% of reading) measures online the O_2 concentration in the outlet gas leaving the cavity. At the outlet from the inner side of the membrane, the gas products (CO/CO_2) are quantified on-line

with a gas analyzer (Emerson X-STREAM XEGP, precision 0.5% of reading) equipped with infrared (IR) sensors. The processing parameters (temperatures, pressures, gas flowrates, outlet gas concentrations) are recorded every seconds by an automated data acquisition system (Beckhoff).

Gas-tight dense MIEC membranes (with tubular shapes) made of ceria enabling favourable diffusion of charge carriers, were synthesized for testing the possibility of isothermal continuous operation, with a spatial separation of the produced O_2 and CO. A series of densified ceria membranes was provided by ALSYS-CTI. They were prepared from a commercial ceria powder (Marion Technologies, ~5-12 µm agglomerates composed of 0.5-2 µm particles), by slip-casting, drying and sintering at 1600°C. The membrane (total length of 150 mm, external diameter of 20 mm, 1.8 mm thick) is a dead-end tube (finger type) fitted with a flange (collar of 32.5 mm diameter) for tight fixation on a water-cooled support. The area of the active membrane exposed to high-temperature solar heat inside the solar-cavity receiver corresponds to 26 cm^2.

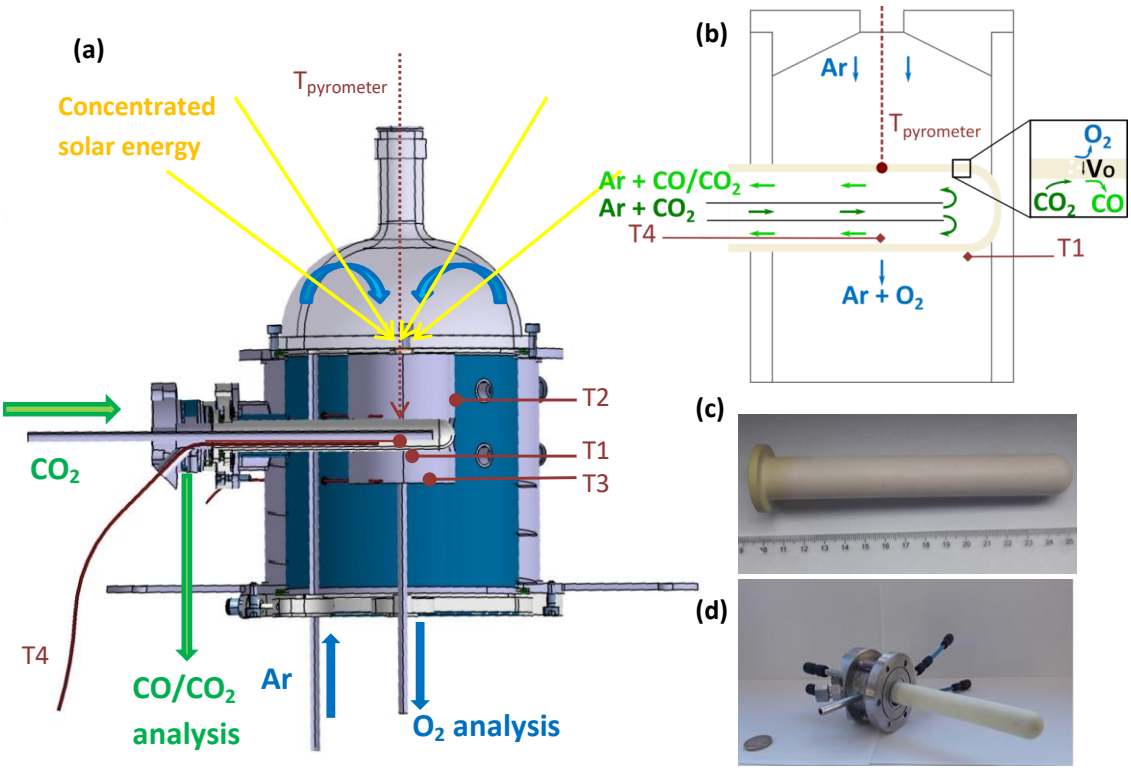

Figure 2: (a) Schematic of the solar membrane reactor for thermochemical splitting of CO_2, (b) principle of *in-situ* separation of CO and O_2 across ceria redox tubular membrane, (c) a tubular ceria membrane, (d) a membrane fixed on the water-cooled support.

3. Results and discussion

In this study, the effects of the operating temperature (1450-1550°C measured by T4), CO_2 mole fraction (25-100%) and CO_2 flow rate on the inner membrane side were studied. The impact of these operating conditions on the O_2 and CO production rates was unravelled.

In order to limit the operating temperature of the membrane, a significant partial pressure gradient was required, with a lower O_2 partial pressure on the reduction side, to favour O_2 release. This was achieved by using a flow of inert gas (Ar, set at 1 NL/min) for the dilution

of O_2 on the outer side of the membrane (alternatively, this could be achieved by reducing the overall pressure thanks to vacuum pumping at the outlet). On the other side, the oxidation reaction of the MIEC material with CO_2 was performed for CO production. Isothermal operation was thus enabled since the both reduction reaction at low partial pressure and the oxidation with CO_2 were carried out at the same temperature. Heat losses can clearly be reduced in such an isothermal processing since temperature swing is avoided, and heat recovery between steps is no longer required.

3.1. Effect of temperature on fuel production performance

The effect of the temperature variation on the dynamic O_2 and CO rate evolution was investigated. During reactor heating, O_2 release was detected from low temperatures (below 900°C) as commonly observed for ceria reduction under inert gas flow. On the inner membrane side, CO_2 was continuously fed during heating but CO production was only detected from ~1400°C, denoting that electronic conductivity and O^{2-} ion migration through the bulk ceria membrane become effective at this temperature, since charge transport in ceria might be viewed as a collaborative movement of electron transfer and ionic migration [34-35]. Cerium oxide can exhibit electronic conduction, ionic conduction, or mixed conduction depending on the oxygen partial pressure, temperature and dopant. The electronic conductivity of ceria vs. p_{O2} has been investigated at temperatures usually below 1000°C [36] and the electrical conductivity has been extrapolated up to 1727°C [37]. At this temperature, the extrapolated electrical conductivity (ions + electrons) of pure ceria is high (85.2 S/m) and decreases when a dopant is added in the structure. Above 700°C, the electronic conductivity of ceria clearly increases when both temperature increases and p_{O2} decreases (following a slope of -1/6 in the $\log \sigma - \log p_{O2}$ plot at 1000°C [36]). However, the p_{O2} dependence of electronic conductivity changes gradually under reducing conditions and it is still unclear if

this electronic conduction behaviour is intrinsic to pure ceria or related to impurities in low concentration [38].

Regarding the dynamics of O_2 and CO evolution, a reproducible pattern was observed consisting of an increase of O_2 production rate when increasing the temperature, followed by the O_2 rate decrease when stabilizing the temperature at a desired value. Concomitantly, the CO rate increased while the O_2 rate decreased until reaching steady-state equilibrium (i.e. CO rate equal to twice the O_2 rate, meaning CO/O_2 ratio = 2). The time to reach equilibrium decreased when increasing the temperature set-point (from 1450 to 1550°C) due to enhanced oxygen diffusivity. It could be further shortened presumably by decreasing the membrane thickness or by changing its chemical composition to enhance oxygen ion diffusion and permeability.

Inversely, when decreasing the temperature set-point, the O_2 production rate was decreased while the CO immediately increased because the oxidation reaction was thermodynamically more favoured. After temperature stabilization, the CO production rate started to decrease steadily to reach a new equilibrium state corresponding to twice the O_2 production rate, while the O_2 increased toward the equilibrium state which settled progressively (due to the temperature decrease that hindered oxygen ion diffusivity, the equilibrium took longer to stabilize). Such typical response patterns illustrate the system dynamics when changing the operating temperature. Figure 3 highlights the above mentioned effect of the decrease in temperature on the transient evolution of O_2 and CO production rates as well as the associated reactor temperatures. The temperatures given by T4 (inside the membrane tube), T1 (below the tube), and $T_{pyrometer}$ (at the tube surface) are very close, whereas T3 (at the cavity bottom) is slightly below T1, and T2 (at the cavity wall) is much lower (~100°C below T3). Figure 3 also plots the O_2 and CO production rates during three temperature dwells after modification of CO_2 flow rate on the oxidation side ($Q_{ox,tot}$) from 1.0 L/min to 0.4 L/min at 1550°C. After

the decrease of $Q_{ox,tot}$, the CO production rate suddenly decreased, due to the less favorable oxidation reaction (this points out the strong influence of the CO_2 feed flow rate on the oxygen transfer rate, as described more in detail in the next section). It should be underlined that after the decrease of $Q_{ox,tot}$, the temperature measured by T4 increased by 10°C, which is attributed to the decrease of convective heat losses. At 1550°C (at T4) with $Q_{ox,tot}$=0.4 L/min, the O_2 flow rate decreased while the CO production rate slightly increased (likely due to the increase of temperature arising when the feed gas flow rate was decreased) up to a steady-state value (0.061 µmol/cm^2/s). Decreasing the temperature to 1500°C (at T4) led to a transient increase of CO production rate (due to thermodynamically favored oxidation reaction) and a decrease of O_2 production rate. Once the temperature was stabilized at 1500°C, the O_2 production rate increased whereas the CO production rate decreased to steady state values. A similar behavior was observed when decreasing the temperature from 1500°C to 1450°C.

When decreasing further the temperature, it can be noticed that complete reoxidation of the ceria membrane occurred when cooling the reactor down to room temperature upon CO_2 flow, due to oxygen replenishment within the ceria lattice via diffusion from the surface. This was confirmed by measuring the total CO amount produced during cooling down, enabling to check the global oxygen balance over the whole solar experiment duration (i.e., total amount of oxygen released during reduction equals to half the total amount of CO produced). During reactor cooling, the oxidation is thermodynamically favoured. However, reoxidation is slow because the reaction is only located at the inner membrane surface. Indeed, the ceria membrane is densified and is not permeable to CO_2 gas, thus offering limited surface area available for the reaction with CO_2.

Regarding the effect of temperature, the CO production rate decreased when decreasing the membrane temperature (~0.061, 0.038, and 0.023 µmol/cm^2/s at 1550, 1500, and 1450°C

respectively, for 100% CO_2 with a flow rate of 0.4 NL/min on the feed side). These flow rates were reached near the equilibration of O_2 and CO production rates in the off-gas. Steady-state productions were not fully reached because the time to reach equilibrium was extended when the operating temperature was decreased (due to reduced mobility of oxygen ions through the membrane) and longer stabilization period would be required. It is expected that the time required for reaching stable production rates could also be reduced by using thinner membranes with enhanced permeability. While this study was rather focused on the dynamic response of the membrane upon changing the operating conditions, full stabilization of the production rates was not targeted given that, as solar tests were performed, it was necessary to manage the allocated on-sun testing period taking into account the meteorological contingencies such as clouds passage.

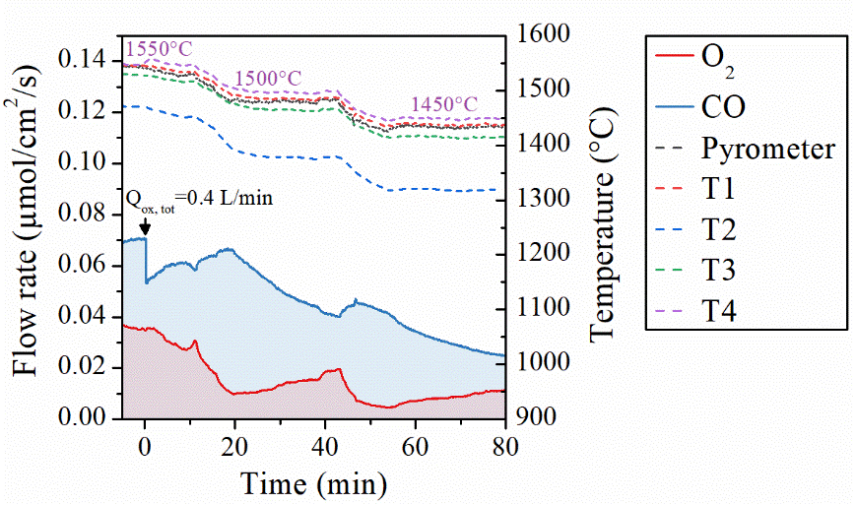

Figure 3: Transient evolution of O_2 and CO production rates along with reactor temperatures, during three temperature dwells at 1550°C, 1500°C and 1450°C (with x_{CO2}=1 and $Q_{ox,tot}$=1 L/min initially at 1550°C, and subsequently decreased to 0.4 L/min).

According to thermodynamic equilibrium of CO_2 thermolysis, the theoretical limit of CO (and O_2) production can be calculated based on the equilibrium constant:

$$K(T) = p_{O2}^{1/2}.p_{CO}/p_{CO2} \quad (4)$$

The value of p_{CO2} at equilibrium, assuming a pure CO_2 feed (inner side), can be obtained from:

$$P_{tot} = p_{CO2} + p_{CO} + p_{O2} \quad (5)$$

where P_{tot} is the total pressure on the inner membrane side under a feed of pure CO_2, and equals 0.9 bar in experiments. The CO partial pressure at equilibrium is obtained by combining Eqs. 4 and 5.

The equilibrium constant K(T) can be tabulated from the enthalpy and entropy changes of the reaction at different temperatures (e.g., $\Delta H°$=279 kJ/mol and $\Delta S°$=84.4 J/K/mol at 1500°C), by using the Gibbs free enthalpy:

$$\Delta G° = \Delta H° - T\Delta S° = -RT.\ln K \quad (6)$$

Since the CO_2 thermolysis is performed via an oxygen-permeable membrane, the controlling driving force is the O_2 partial pressure (p_{O2}) on the outer reduction side of the membrane (Ar sweep side), thus determining the chemical potential gradient. Assuming that p_{O2} at equilibrium on the inner side corresponds to p_{O2} in the Ar feed on the reduction side ($p_{O2}=10^{-5}$ bar), the gas composition resulting from CO_2 thermolysis in the membrane reactor can be calculated and regarded as the thermodynamic limit.

The logarithm of the steady-state gas production rates (O_2 and CO) was plotted versus the reverse temperature (Figure 4) and it follows a linear trend according to the Arrhenius expression. The activation energies calculated for CO and O_2 productions (in the range 1450-

1550°C) are 255 and 271 kJ/mol respectively, compared to ~270 kJ/mol for the theoretical value provided by the thermodynamic limit (close to the reaction enthalpy of CO_2 thermolysis). The values obtained experimentally are clearly in line with the theoretical value, demonstrating that the reaction conditions allow approaching thermodynamic equilibrium.

The theoretical CO_2 conversion can be evaluated by considering the maximum CO production rate at thermodynamic equilibrium (represented in Figure 4). For instance at 1500°C, with p_{O2}=1.10^{-5} bar on the Ar sweep side and $Q_{ox,tot}$=0.4 L/min on the CO_2 feed side, the theoretical maximum CO_2 conversion would be ~4.7% (versus 2.7% at 1450°C and 7.6% at 1550°C).

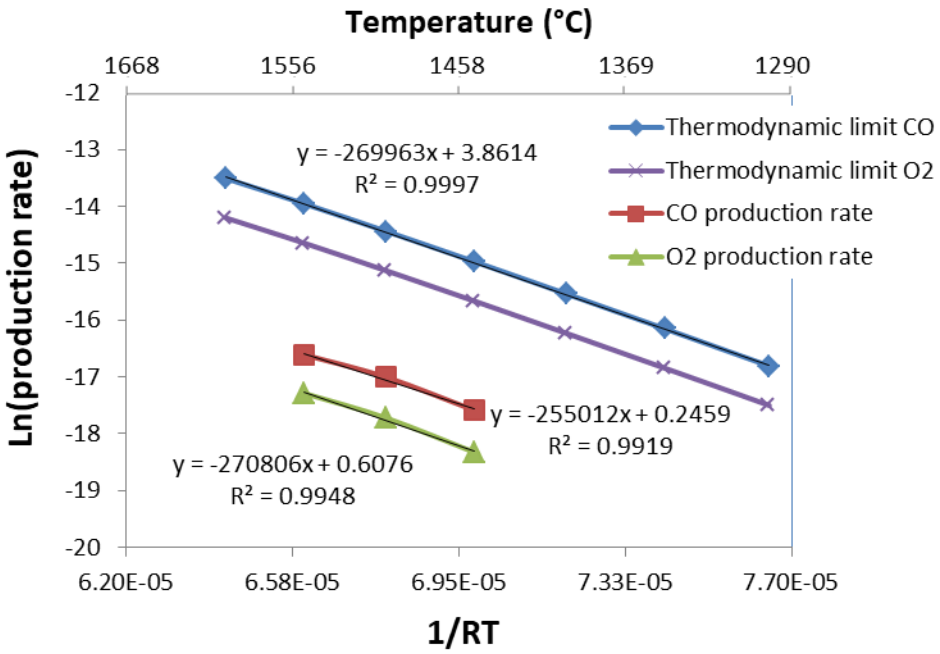

Figure 4: Arrhenius plot of the steady-state gas production rates measured experimentally compared with the theoretical thermodynamic limit (with p_{O2}=1.10^{-5} bar on the Ar sweep side, $Q_{ox,tot}$=0.4 L/min on the CO_2 feed side).

3.2. Effect of CO_2 flow rate and CO_2 mole fraction on membrane performance

The maximum CO flow rate of 0.071 µmol/cm^2/s (and O_2 flow rate of 0.035 µmol/cm^2/s) was achieved at 1550°C with a volumetric CO_2 flow rate increased to 1 NL/min, which denotes that the amount of CO_2 fed is also a key parameter controlling fuel production. Indeed, the quantity of CO_2 affects the mass transfer at the membrane surface, as well as the CO/CO_2 ratio which controls the thermodynamic driving force. High gas flow rates favor mass transfer, dilution of products and their continuous removal from the reaction site, thus shifting the equilibrium towards the production of CO. Conversely, relatively low gas flow rates are not suitable to sweep away the products from both sides of the membrane, thus inducing mass transfer limitations. On the other hand, a high CO_2 feed rate comes at the expense of the quantities of unreacted CO_2 leaving the reactor together with the CO produced.

Given the low CO_2 conversion that remains below 1% (because CO_2 is fed in excess), the outlet gas contains a flow of CO diluted in CO_2. A downstream separation of the produced CO with recycling of the unconverted CO_2 fraction at the process inlet is thus required. Typical CO_2 conversions increase from ~0.3% to 0.5% when decreasing the inlet CO_2 flow rate from 1 to 0.4 L/min. The development of dual-membrane reactors for *in-situ* removal of both O_2 and CO produced by CO_2-thermolysis could be an option for tuning fuel purity. This requires the development of a membrane able to extract the produced CO from the CO_2-rich stream. Otherwise the CO must be separated from the CO_2 stream at the reactor outlet and the captured CO_2 can be re-injected to the reactor inlet.

Upon changing the gas flow rates, the dynamic response of CO and O_2 evolution was also determined. Figure 5a shows the CO and O_2 mole fractions after changing the inlet CO_2 flow rate ($Q_{ox,tot}$) from 0.4 to 1.0 L/min. The CO concentration decreases sharply due to the total flow rate increase while the O_2 concentration increases steadily. Figure 5b illustrates the

transient O_2 and CO production rates at 1500°C with x_{CO2}=1.00 after modification of $Q_{ox,tot}$ from 0.4 to 1.0 L/min with similar x_{CO2} and temperature. The increase of CO_2 flow rate results in an increase of both the O_2 and CO production rates (from 0.020 to 0.026 µmol/cm^2/s for O_2 and from 0.039 to 0.053 µmol/cm^2/s for CO at 1500°C). This is because the CO dilution is enhanced and the CO/CO_2 ratio decreases, which in turn promotes the CO_2 dissociation reaction. During ~40 s after the change of $Q_{ox,tot}$ value, a difference exists between the gas flow rate input in the membrane and the outlet gas flow rate analyzed (Figure 5a), due to the volume swept between the gas flow controller and the gas analyzer. Once the inlet gas has totally filled the membrane reactor volume, the outlet CO concentration drops due to dilution effect when increasing the inlet gas flow rate to 1.0 L/min. The CO_2 flow sweeping the inner side of the membrane is assumed to approach a plug flow model given the tubular geometry of the system. This is evidenced by the steep step in the CO concentration resulting from the stepwise increase of the inlet gas flow rate (Figure 5a). Two distinct periods can be observed. In the first period, the gas concentration analyzed at the outlet corresponds to the previous $Q_{ox,tot}$ due to time lag (hatched area in Figure 5b). The second period corresponds to a continuous increase of the gas flow rate from initial to final total gas flow rate (grey area in Figure 5b). In this case, it was assumed that the gas flow rate increased linearly from 0.4 to 1.0 L/min to smooth the change in CO concentration due to the change of the inlet gas flow rate. The CO production rate starts to increase 30 s after $Q_{ox,tot}$ change (grey area). This sharp increase is attributed to the re-oxidation of the membrane material due to the CO/CO_2 ratio decrease and to the enhancement of oxidant gas access to the reactive surface, favoring CO product removal. Then, the CO production rate slowly decreases to reach a stable value after ~5-6 min. In parallel, the O_2 production rate increases smoothly to the stabilized value, highlighting an enhanced oxygen transfer due to $Q_{ox,tot}$ increase. It can be noticed that the O_2 production rate starts to decrease for a short period (time: 30-60s), due to the slight

temperature decrease when the CO_2 flow rate is increased from 0.4 to 1 L/min (Figure 5b). Indeed, increasing the feed gas flow rate ($Q_{ox,tot}$) in the membrane also leads to a decrease of temperature inside the membrane (T4 decreases by 16°C), given that the energy required to heat the injected gas increases. Concomitantly, the temperature at the membrane outside presents a slight decrease (7°C and 6°C for temperatures measured by the pyrometer and by T1, respectively). Therefore, the temperatures measured by the pyrometer, by T1 and by T4 become very similar when $Q_{ox,tot}$=1.0 L/min.

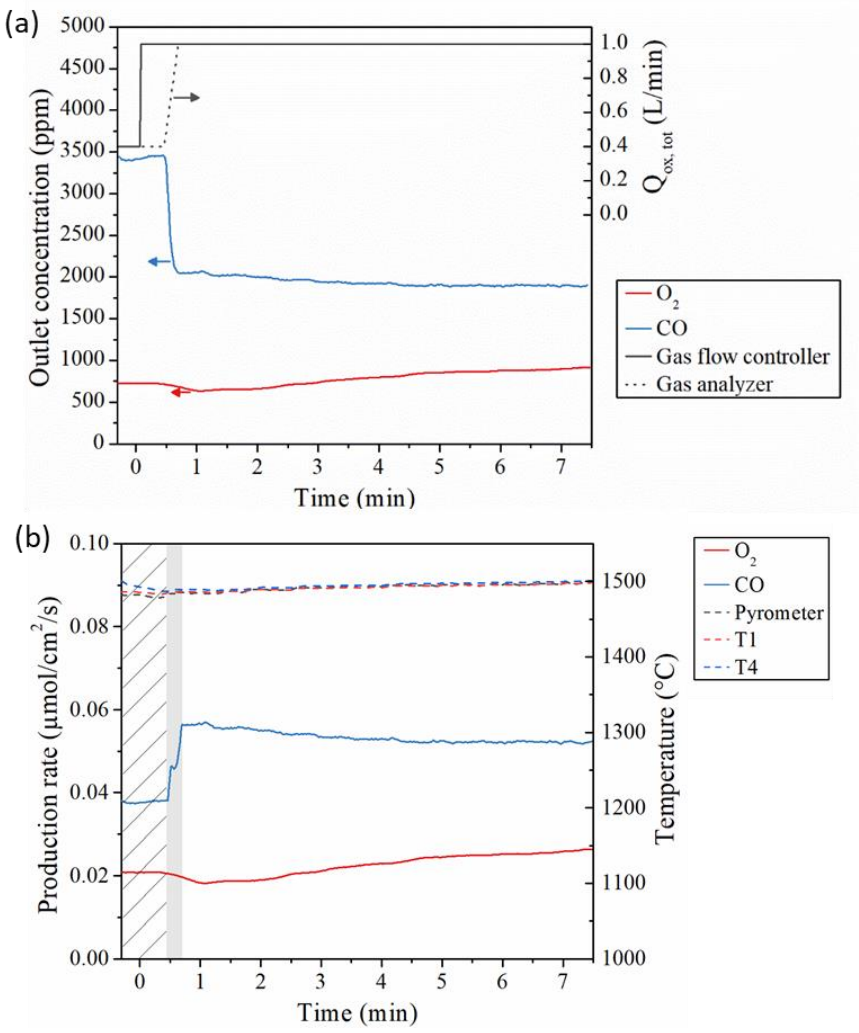

Figure 5: Effect of a change in the feed gas flow rate on the evolution of: (a) O_2 and CO proportions, along with $Q_{ox,tot}$ in the gas flow controller (solid grey line) and in the gas analyzer (dotted grey line), and (b) O_2 and CO production rates (solid lines), along with the

temperatures (dashed lines) for ceria membrane (at 1500°C with x_{CO2}=1.00 and $Q_{ox,tot}$ fixed at 1.00 L/min after being increased from 0.4 L/min).

Finally, the effect of inlet CO_2 mole fraction (x_{CO2} = 0.25, 0.50, 1.00) was investigated while keeping constant the total gas flow rate on the oxidation side (0.4 NL/min balanced with Ar) at 1500°C. The CO production rate decreased when decreasing the CO_2 mole fraction (0.037, 0.027, and 0.020 µmol/cm^2/s for CO_2 mole fraction of 1.00, 0.50, and 0.25 respectively). The O_2 production rate thus also concomitantly decreased, following a smooth evolution (0.019, 0.013, and 0.010 µmol/cm^2/s respectively). This result points out the strong influence of the oxidant mole fraction on the fuel production rate. This is again because a lowered CO/CO_2 ratio (by increasing either CO_2 flow-rate or CO_2 mole fraction) thermodynamically shifts the oxidation reaction towards CO production. Figure 6 illustrates the effect of varying the CO_2 mole fraction on the dynamic evolution of both CO and O_2 production rates, as well as reactor temperatures during solar heating to 1500°C. The O_2 detection started when T4 and T1 exceeded around 800°C (the temperature of the membrane outer surface, directly exposed to radiation, should potentially be higher). The O_2 production rate reached a maximum during the ceria membrane reduction and then declined upon temperature stabilization at 1500°C to level off when approaching equilibrium. Concomitantly, the CO production started to increase from ~1400°C (measured at T4) and reached a stable equilibrium value once the temperature was stabilized at 1500°C. When decreasing the inlet CO_2 mole fraction, the CO production first dropped suddenly because of the less favorable oxidation reaction, and then rose steadily to approach equilibrium with the O_2 evolved on the opposite membrane side.

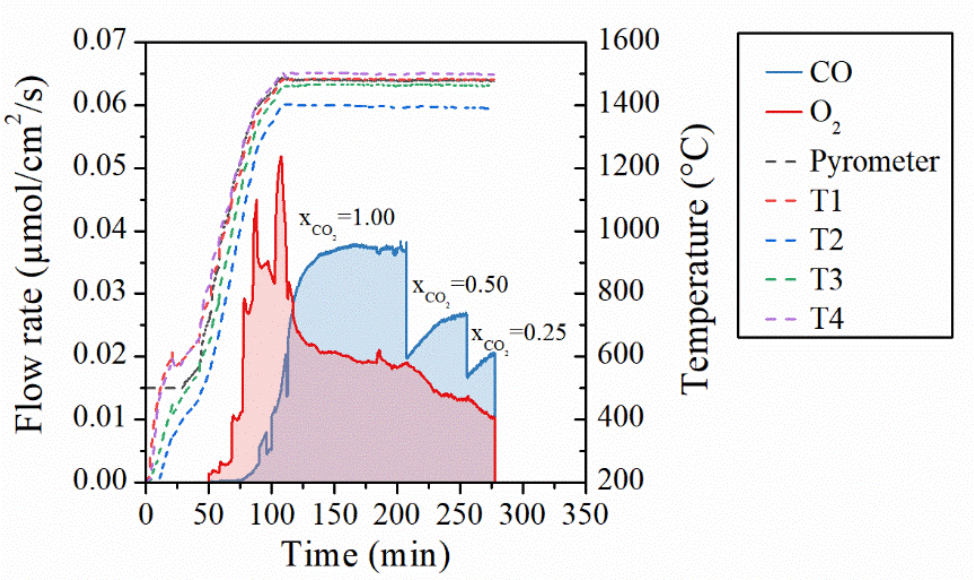

Figure 6: Transient evolution of O_2 and CO production rates along with reactor temperatures, when the inlet CO_2 mole fraction decreases from 1.00 to 0.25 (at 1500°C with $Q_{ox,\,tot}$=0.4 L/min).

In summary, unprecedented fuel production rates were achieved in the developed solar membrane reactor by tuning the operating conditions during isothermal CO_2 splitting. Among the investigated parameters, the temperature, the inlet CO_2 mole fraction and the inlet CO_2 flow rate (both affecting the CO dilution and the p_{CO}/p_{CO2} ratio) showed significant effect. Since the temperature cannot be further increased due to materials limitations, the tuning of gas flow conditions are possible options to improve CO production while preserving the membrane stability. Interestingly, the specific CO and O_2 production rates per unit area of membrane increased when increasing either the inlet CO_2 mole fraction or the volumetric CO_2 flow rate on the inner side of the membrane. Such results arise from enhanced mass transfer at the membrane surface, higher CO product dilution (or lower p_{CO}/p_{CO2} ratio) and a thermodynamically favored reaction.

3.3. Membrane stability and global CO_2-splitting performance assessment

The membrane reactor was operated during full day of continuous on-sun operation, representing a total duration of ~7.5 h under concentrated solar radiation. The membrane morphology after solar thermolysis experiments under CO_2 exposure, was characterized using scanning electron microscopy (SEM). Figure 7 shows SEM images of the membrane (surface and cross-section) after CO_2 splitting in the solar reactor. A microstructural evolution of the ceria membrane was evidenced after utilization in the solar reactor at ~1550°C (or higher for the irradiated surface parts). Indeed, the ceria grain size (estimated by image analysis) increased from 3-10 µm initially to 8-30 µm after reaction, suggesting a membrane sintering in the solar reactor. This means that a higher calcination temperature of the membrane could be used for microstructure stabilization, with limited grain growth during solar processing. Importantly, only closed (non-interconnected) pores were detected in the membrane cross-section after cycling, without any visible defects or cracks in the observed areas. This suggests that the diffusion of molecular gas species (through the pores/defects) was not favored during the tests and mass transfer occurred via diffusion of O^{2-} ions through the crystal lattice vacancies. In order to limit the impact of any potential gas leakage across the membrane, experiments were performed by applying an equal total pressure (~0.9 bar) on both membrane sides.

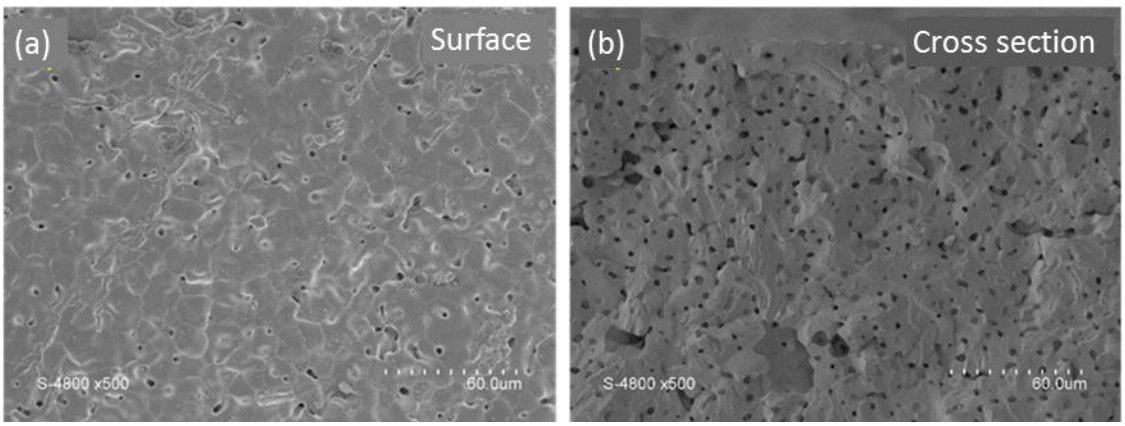

Figure 7: SEM images of (a) outside surface and (b) cross-section of the ceria membrane after CO_2 splitting under concentrated solar radiation (during ~7.5h at 1450-1550°C).

The membrane thermal stability under continuous solar testing was addressed by operating the membrane at the same conditions for several hours. Any evolution of membrane performance over time may be considered as an indication of a microstructural evolution of the material (sintering/defects). The O_2 and CO production rates were measured at 1500°C (with x_{CO2}=1 and $Q_{ox,tot}$=0.4 L/min) after about 3, 5, and 6 hours of operation times. The corresponding O_2 production rates were 0.019, 0.020, and 0.019 µmol/cm^2/s, while the CO production rates were 0.037, 0.041, and 0.038 µmol/cm^2/s, thus confirming membrane reactor performance stability under real solar irradiation conditions.

The obtained fuel production rates outperformed the maximum values currently reported in the literature by up to ~10 times, using the manufactured ceria membranes operated up to ~1550°C with oxidation under 100% CO_2 on the feed side. Figure 8 compares the O_2 and CO production rates achieved in the novel solar membrane reactor with previously reported data using an indirectly-heated tubular ceria membrane [17]. The main reasons explaining the superior performance obtained in the new developed solar reactor are presumably the higher gas flow rates used on both sides of the membrane (around one order of magnitude higher for Ar and CO_2), as well as the microstructure of the densified membranes exhibiting low porosity, closed pores and negligible permeability for molecular gas species. In contrast, some transfer of molecular gas species through the membrane was presumed in the work of Tou et al. [17-18], in which gas tightness issues were clearly pointed out [39]. This transfer of molecular gas species (Ar and CO_2) between the sweep and feed membrane sides could potentially be favored by the thin membrane wall thickness (0.5 mm [17]), combined with an

asymmetric pore structure (large finger-like pores in the cross-section) resulting from the phase-inversion synthesis method, which could in turn favor interconnected pores/defects and might contribute to lower the performance.

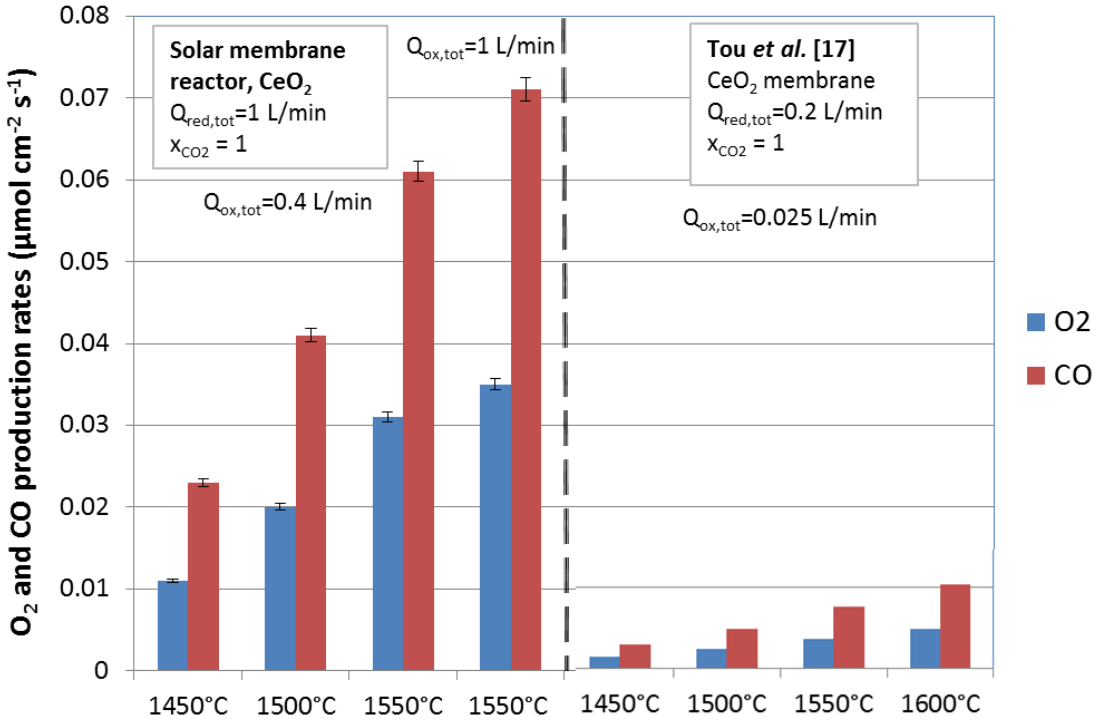

Figure 8: Comparison of O_2 and CO production rates obtained in ceria membrane reactors, in this work and in the literature by Tou et al. [17].

This study thus showed the feasibility of continuous CO_2 splitting in the solar membrane reactor under real concentrated sunlight. The results confirmed that ceria symmetric membrane offers good oxygen permeability as well as suitable thermal stability at temperatures up to 1550°C. In presence of the membrane, CO production from CO_2 thermolysis at 1500-1550°C is enhanced by several orders of magnitude compared to homogeneous thermolysis, which is negligible at these temperatures [6]. Adding Ar inert gas

flow to the sweep side revealed suitable to remove permeated oxygen and to displace the dissociation equilibrium to the products side. Such continuous oxygen extraction favorably shifts the equilibrium-limited CO_2 splitting reaction towards fuel production. Further attempts to promote oxygen-ion transport across the semi-permeable dense membrane should be pursued. Alternative materials for the membrane such as doped ceria or perovskites (or dual-phase membranes) could be explored because they exhibit enhanced oxygen ion diffusivity at lower processing temperatures, which thereby should favor the thermochemical and structural stability of the reactive membrane [40-42]. As the rate limiting process is likely oxygen transfer at the interfaces, the increase of the active surface area should be beneficial to favor both CO_2 adsorption and oxygen extraction on the sweep side. The use of thin membranes on porous substrates was investigated for low temperatures applications and could be further applied to the solar reactor [43-45]. For example, with the addition of a porous layer of perovskite material on both sides to increase the number of adsorption/desorption sites, the CO production rate is expected to rise.

In addition, the effect of membrane thickness, oxygen-ion transport rate, pressure gradient between the two membrane sides, inert gas and oxidant flow rates on the membrane reactor performance will need to be investigated and optimised in future studies.

4. Conclusion

This study focused on the design and development of a membrane solar reactor for continuous CO_2 splitting and isothermal operation with *in-situ* O_2 removal across a MIEC ceria membrane. The solar membrane reactor was reliably operated during continuous on-sun operation with remarkable thermochemical CO_2 splitting performance. The highest CO production rate reached 0.071 μmol/cm^2/s at 1550°C with pure CO_2 on the feed side and Ar

(p_{O2}~10^{-5} bar) on the sweep side, thus outperforming by a factor of about x10 the maximum performance reported to date for CO_2 thermolysis at the same membrane temperature. A temperature increase from 1450 to 1550°C strongly promoted the O_2 and CO generation rates. Increasing the total CO_2 flow rate or CO_2 mole fraction both improved CO product dilution (lower CO/CO_2 ratio) and gas products removal. This led to shifting the thermodynamic equilibrium to the products side while enhancing mass transfer (i.e., CO_2 access to reactive sites), in turn promoting the overall fuel production rate. Attractive results were thus obtained during this first-ever demonstration of such a solar-driven membrane reactor concept. Although not studied here, the analogous direct H_2O splitting into separate streams of H_2 and O_2 could also be achieved with the same reactor. There is still room for improvement with regard to both the specific rate of fuel production per unit area of reactive membrane and the stability of the membrane during thermal cycling (day/night cycle with heating/cooling steps during start and end of solar operation). The permeability of oxygen (by ionic migration) could be boosted by using other relevant MIEC materials such as perovskites, exhibiting enhanced diffusion capabilities at lower temperatures (below 1400°C), thereby reducing the thermal stress imposed to the redox membrane material. In addition, the deposition of a thin dense MIEC membrane on a porous redox support can be another option to optimize the oxygen transfer while enhancing the active surface area of the redox material. Therefore, the utilization of more active oxygen-conducting redox materials, improved membrane designs, and their implementation in solar reactors are important requirements to encourage further expansion of solar fuels production by this innovative approach.

Acknowledgments

This work was funded by the French National Agency for Research (ANR, SUNFUEL project, contract N°ANR-16-CE06-0010). The authors thank R. Garcia (PROMES) for solar reactor design, J. Jouannaux (IEM) for SEM observations, B. Cartoixa and V. Bollee (Alsys-CTI) for supplying the tubular ceria membranes.

References

[1] G. Centi, S. Perathoner, Opportunities and prospects in the chemical recycling of carbon dioxide to fuels. *Cat. Today*, 148 (2009) 191-205.

[2] C. Graves, S.D. Ebbesen, M. Mogensen, K.S. Lackner, Sustainable hydrocarbon fuels by recycling CO_2 and H_2O with renewable or nuclear energy. *Renewable and Sustainable Energy Reviews*, 15 (2011) 1-23.

[3] B. Hua, C. Guild, S. L. Suib, Thermal, electrochemical, and photochemical conversion of CO_2 to fuels and value-added products, *J. CO_2 Utilization*, 1 (2013) 18–27.

[4] D. Yadav, R. Banerjee, A review of solar thermochemical processes, Renewable and Sustainable Energy Reviews, 54 (2016) 497–532.

[5] S. Chuayboon, S. Abanades, An overview of solar decarbonization processes, reacting oxide materials and thermochemical reactors for hydrogen and syngas production, *Int. J. Hydrogen Energy*, 45(48) (2020) 25783-25810.

[6] S. Abanades, Metal oxides applied to thermochemical water-splitting for hydrogen production using concentrated solar energy, *ChemEngineering*, 3(3) (2019) 63. DOI: 10.3390/chemengineering3030063

[7] P.R. Yaashikaa, P. Senthil, Kumar, Sunita J. Varjani, A. Saravanan, A review on photochemical, biochemical and electrochemical transformation of CO_2 into value-added products, *J. CO_2 Utilization*, 33 (2019) 131-147.

[8] Y. Lu, L. Zhu, C. Agrafiotis, J. Vieten , M. Roeb, C. Sattler, Solar fuels production: Two-step thermochemical cycles with cerium-based oxides, *Progress in Energy and Combustion Science*, 75 (2019) 100785.

[9] A. Haeussler, S. Abanades, J. Jouannaux, M. Drobek, A. Ayral, A. Julbe, Recent progress on ceria doping and shaping strategies for solar thermochemical water and CO_2 splitting cycles, *AIMS Materials Science*, 6(5) (2019) 657-684.

[10] A. Haeussler, S. Abanades, J. Jouannaux, A. Julbe, Non-stoichiometric redox active perovskite materials for solar thermochemical fuel production: a review, *Catalysts*, 8(12) (2018) 611. doi: 10.3390/catal8120611

[11] A. Trovarelli, Catalytic properties of ceria and CeO_2-containing materials. *Catal. Rev.*, 38 (1996) 439-520.

[12] W. Li, X. Zhu, Z. Cao, W. Wang, W. Yang, Mixed ionic-electronic conducting (MIEC) membranes for hydrogen production from water splitting, *Int. J. Hydrogen Energy*, 40 (2015) 3452-3461.

[13] L. Zhu, Y. Lu, S. Shen, Solar fuel production at high temperatures using ceria as a dense membrane, *Energy*, 104 (2016) 53-63.

[14] X.-Y. Wu and A. F. Ghoniem, Mixed ionic-electronic conducting (MIEC) membranes for thermochemical reduction of CO_2: A review, *Prog. Energy Combust. Sci.*, 74 (2019) 1–30, doi: 10.1016/j.pecs.2019.04.003.

[15] N. Itoh, M. A. Sanchez, W.-C. Xu, K. Haraya, and M. Hongo, Application of a membrane reactor system to thermal decomposition of CO_2, *J. Membr. Sci.*, 77(2–3) (1993) 245–253, doi: 10.1016/0376-7388(93)85073-6.

[16] H. Naito, Hydrogen production from direct water splitting at high temperatures using a ZrO_2-TiO_2-Y_2O_3 membrane, *Solid State Ionics*, 79 (1995) 366–370, doi: 10.1016/0167-2738(95)00089-O.

[17] M. Tou, R. Michalsky, and A. Steinfeld, Solar-driven thermochemical splitting of CO_2 and in situ separation of CO and O_2 across a ceria redox membrane reactor, *Joule*, 1(1) (2017) 146–154, doi: 10.1016/j.joule.2017.07.015.

[18] M. Tou, J. Jin, Y. Hao, A. Steinfeld, and R. Michalsky, Solar-driven co-thermolysis of CO_2 and H_2O and in-situ oxygen removal across a non-stoichiometric ceria membrane, *React. Chem. Eng.*, 4 (2019) 1431, doi: 10.1039/C8RE00218E.

[19] S. Smart, S. Liu, J.M. Serra, A. Basile, J.C. Diniz da Costa, Perovskite membrane reactors: fundamentals and applications for oxygen production, syngas production and hydrogen processing. Membranes for Clean and Renewable Power Applications. (pp. 182-234) edited by Annarosa Gugliuzza and Angelo Basile. Sawston, Cambridge, United Kingdom: Woodhead Publishing. (2014). doi: 10.1533/9780857098658.3.182

[20] X. Dong, W. Jin, N. Xu, and K. Li, Dense ceramic catalytic membranes and membrane reactors for energy and environmental applications, *Chem. Commun.*, 47(39) (2011) 10886, doi: 10.1039/c1cc13001c.

[21] W. Fang, F. Steinbach, Z. Cao, X. Zhu, and A. Feldhoff, A Highly Efficient Sandwich-Like Symmetrical Dual-Phase Oxygen-Transporting Membrane Reactor for Hydrogen Production by Water Splitting, *Angew. Chemie Int. Ed.*, 55(30) (2016) 8648–8651.

[22] U. (Balu) Balachandran, T. H. Lee, and S. E. Dorris, Hydrogen production by water dissociation using mixed conducting dense ceramic membranes, *Int. J. Hydrogen Energy*, 32(4) (2007) 451–456.

[23] X. Y. Wu, L. Chang, M. Uddi, P. Kirchen, and A. F. Ghoniem, Toward enhanced hydrogen generation from water using oxygen permeating LCF membranes, *Phys. Chem. Chem. Phys.*, 17(15) (2015) 10093–10107.

[24] J. Sunarso, S. Baumann, J.M. Serra, W.A. Meulenberg, S. Liu, Y.S. Lin, J.C. Diniz da Costa, Mixed ionic-electronic conducting (MIEC) ceramic-based membranes for oxygen separation, *J. Membr. Sci.*, 320(1–2) (2008) 3–41.

[25] U. Balachandran, J. T. Dusek, and S. M. Sweeney, Methane to syngas via ceramic membranes, *Am. Ceram. Soc. Bull.*, 74 (1995) 71–75.

[26] Z. Gong and L. Hong, Integration of air separation and partial oxidation of methane in the $La_{0.4}Ba_{0.6}Fe_{0.8}Zn_{0.2}O_{3-\delta}$ membrane reactor, *J. Membr. Sci.*, 380(1–2) (2011) 81–86, doi: 10.1016/j.memsci.2011.06.033.

[27] H. Jiang, H. Wang, S. Werth, T. Schiestel, and J. Caro, Simultaneous Production of Hydrogen and Synthesis Gas by Combining Water Splitting with Partial Oxidation of Methane in a Hollow-Fiber Membrane Reactor, *Angew. Chem. Int. Ed.*, 47(48) (2008) 9341–9344, doi: 10.1002/anie.200803899.

[28] A. Evdou, V. Zaspalis, and L. Nalbandian, $La_{1-x}Sr_xFeO_{3-\delta}$ perovskites as redox materials for application in a membrane reactor for simultaneous production of pure hydrogen and synthesis gas, *Fuel*, 89(6) (2010) 1265–1273.

[29] L. Nalbandian, A. Evdou, V. Zaspalis, $La_{1-x}Sr_xMO_3$ (M = Mn, Fe) perovskites as materials for thermochemical hydrogen production in conventional and membrane reactors, *Int. J. Hydrogen Energy*, 34 (2009) 7162–7172.

[30] A. Haeussler, S. Abanades, A. Julbe, J. Jouannaux, M. Drobek, A. Ayral, B. Cartoixa, Remarkable performance of microstructured ceria foams for thermochemical splitting of H_2O and CO_2 in a novel high-temperature solar reactor, *Chem. Eng. Res. Des.*, 156 (2020) 311-323. DOI: 10.1016/j.cherd.2020.02.008

[31] A. Haeussler, S. Abanades, A. Julbe, J. Jouannaux, and B. Cartoixa, Solar thermochemical fuel production from H_2O and CO_2 splitting via two-step redox cycling of reticulated porous ceria structures integrated in a monolithic cavity-type reactor, *Energy*, 201 (2020) 117649, doi: 10.1016/j.energy.2020.117649.

[32] A. Haeussler, S. Abanades, A. Julbe, J. Jouannaux, and B. Cartoixa, Two-step CO_2 and H_2O splitting using perovskite-coated ceria foam for enhanced green fuel production in a porous volumetric solar reactor, *Journal of CO_2 Utilization*, 41 (2020) 101257, doi: 10.1016/j.jcou.2020.101257.

[33] A. Haeussler, S. Abanades, F. A. Costa Oliveira, M. A. Barreiros, A.P.F. Caetano, R. M. Novais, R. C. Pullar, Solar redox cycling of ceria structures based on fiber boards, foams and biomimetic cork-derived ecoceramics for two-step thermochemical H_2O and CO_2 splitting, *Energy & Fuels*, 34(7) (2020) 9037–9049.

[34] J. J. Plata, A. M. Márquez, J. Fdez. Sanz, Electron Mobility via Polaron Hopping in Bulk Ceria: A First-Principles Study, *The Journal of Physical Chemistry C*, 117(28) (2013) 14502-14509, doi: 10.1021/jp402594x.

[35] J. J. Plata, A. M. Márquez, J. Fdez. Sanz, Transport Properties in the CeO_{2-x}(111) Surface: From Charge Distribution to Ion-Electron Collaborative Migration, *The Journal of Physical Chemistry C*, 117(48) (2013) 25497-25503, doi: 10.1021/jp4066532.

[36] Y.P. Xiong, H. Kishimoto, K. Yamaji, M. Yoshinaga, T. Horita, M.E. Brito, H. Yokokawa, Electronic Conductivity of CeO_2: Its Dependence on Oxygen Partial Pressure and Temperature, *Electrochem. Solid-State Lett.*, 13 (2010) B21.

[37] K.-S. Kwong, R.C. Woodside, B.L. Wright, M.J.M. Johnson, Electrical Conductivity of Ceria Electrodes for Use in MHD Generators, *Proc. 39th International Conference and Expo on Advanced Ceramics and Composites*, Daytona Beach, FL 1/25/2018 - 1/30/2018- United States. https://www.osti.gov/servlets/purl/1562265

[38] Y.P. Xiong, H. Kishimoto, K. Yamaji, M. Yoshinaga, T. Horita, M.E. Brito, H. Yokokawa, Electronic conductivity of pure ceria, *Solid State Ionics*, 192(1) (2011) 476-479.

[39] M. Tou, A Membrane Reactor for the Solar Thermolysis of CO_2 and H_2O: A Thermodynamic and Experimental Analysis, Doctoral dissertation, ETH Zurich, 2019. https://doi.org/10.3929/ethz-b-000332855.

[40] J. H. Joo, K. S. Yun, J. H. Kim, Y. Lee, C. Y. Yoo, and J. H. Yu, Substantial Oxygen Flux in Dual-Phase Membrane of Ceria and Pure Electronic Conductor by Tailoring the Surface, *ACS Appl. Mater. Interfaces*, 7(27) (2015) 14699–14707.

[41] A. Belzner, T. M. Gür, and R. A. Huggins, Oxygen chemical diffusion in strontium doped lanthanum manganites, *Solid State Ionics*, 57(3–4) (1992) 327–337.

[42] K. S. Lee, S. Lee, J. W. Kim, and S. K. Woo, Enhancement of oxygen permeation by $La_{0.6}Sr_{0.4}CoO_{3-\delta}$ coating, *Desalination*, 147(1–3) (2002) 439–444.

[43] X.-Y. Y. Wu, A. F. Ghoniem, and M. Uddi, Enhancing co-production of H_2 and syngas via water splitting and POM on surface-modified oxygen permeable membranes, *AIChE J.*, 62(12) (2016) 4427–4435.

[44] P. Lemes-Rachadel, G. S. Garcia, R. A. F. Machado, D. Hotza, and J. C. D. Da Costa, Current developments of mixed conducting membranes on porous substrates, *Mater. Res.*, 17(1) (2014) 242–249.

[45] P. M. Geffroy, A. Vivet, L. Guironnet, N. Richet, F. Rossignol, and T. Chartier, Perovskite foams used in combination with dense ceramic membranes for oxygen transport membrane applications, *Ceram. Int.*, 44(16) (2018) 19831–19835.